Dose-Modulated Maskless Lithography for the Efficient Fabrication of Compound Eyes With Enlarged Field-of-View
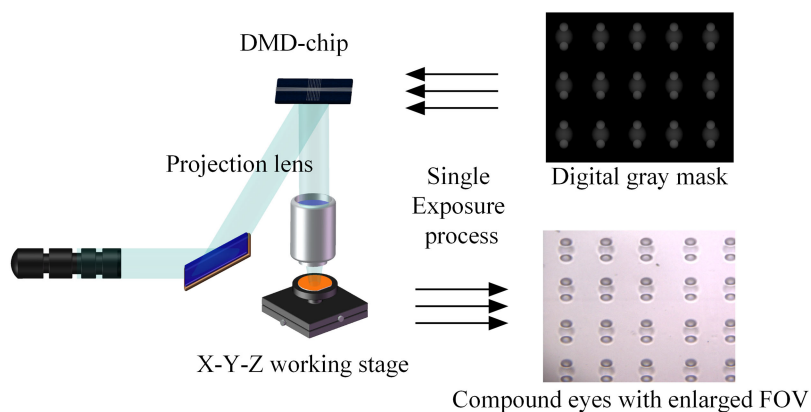
Jianghui Liu
Junbo Liu
Qingyuan Deng
Xi Liu
Yu He
Yan Tang
Song Hu

DMD-chip

Projection lens

Single Exposure process

Digital gray mask

X-Y-Z working stage

Compound eyes with enlarged FOV

Dose-Modulated Maskless Lithography for the Efficient Fabrication of Compound Eyes With Enlarged Field-of-View

Jianghui Liu,[1,2] **Junbo Liu** [ID],[1] **Qingyuan Deng,**[3] **Xi Liu,**[1,2] **Yu He,**[1] **Yan Tang,**[1] **and Song Hu**[1]

[1]State Key Laboratory of Optical Technologies on Nano-fabrication and Micro-Engineering, Institute of Optic and Electronics, Chinese Academy of Sciences, Chengdu 610729, China
[2]University of Chinese Academy of Sciences, Beijing 100049, China
[3]School of Automation, Chongqing University of Posts and Telecommunications, Chongqing 400065, China

Abstract: In this paper, a method of dose-modulated maskless lithography (DMML) with high efficiency for the fabrication of a special compound-eyes array with enlarged field-of-view is proposed. Before the fabrication process, practical measurements were primarily conducted to quantify the dose-modulated effect. Next, a digital gray pattern, generated according to the required exposure dose distribution of the design structure, was adopted as a virtual mask to modulate the exposure depth point-by-point. In this way, the whole exposure process requires only one-step. Besides, because the DMML uses sequential gray-levels to modulate the exposure depth, the fabricated structure has a more continuous profile surface. Combined with the thermal reflow process, and the pattern reversion process, the compound eyes array was transferred to the planar polydimethylsiloxane films with high quality. Subsequent tests reveal that the physical performance of fabricated compound eyes array, including the surface profile and the rotated orientation, has a good agreement with our design.

Index Terms: Maskless lithography, dose modulation, compound eyes, FOV.

1. Introduction

Natural insect eyes with special structures typified by dragon-fly [1], [2], arthropod [3] and fruit fly [4] have become an attractive research due to their preeminent abilities such as low aberration [5], moving detection [6], and wide FOV [7], etc. These compound eyes are usually made up of thousands of small close-connected lens arranged on spherical surface [8], [9]. Micro optical devices inspired by natural compound eyes show prominent function in various field such as imaging system [10], antireflection materials [11], and medical instruments [12], etc.
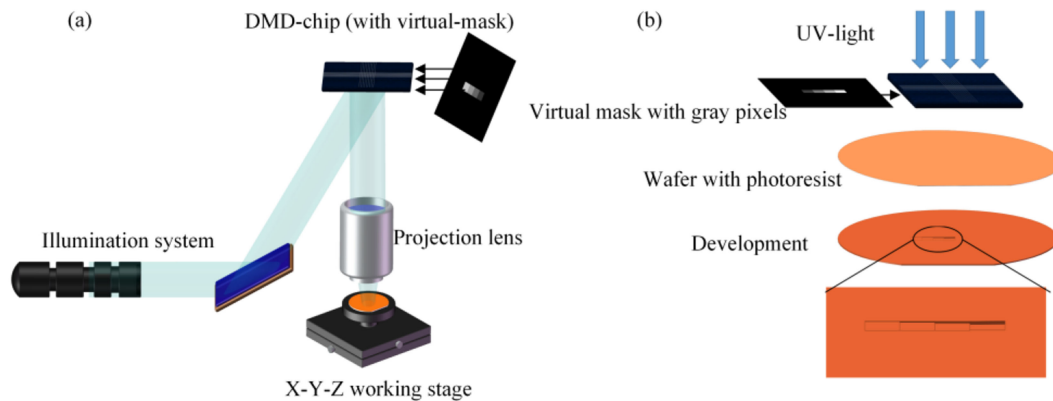
Fig. 1. The sketch of DMML. (a) The basic setups of lithography. (b) The exposure process based on dose modulation.

Since the outstanding abilities and wide applications these compound eyes have, much attempts have been paid to the fabrication methods of such biomimetic structures. Conventionally, the existing routes prevailingly comprise the nanoimprint [13], soft lithography [14], and moving mask exposure [15], etc. Micro compound eyes fabricated by the aforementioned methods exhibit special function. However, a common feature leaded by the planar substrate of such compound eye arrays is the lack of FOV. To solve this issue, on the basics of such fabrication methods, several supplementary methods such as the thermomechanical deformation [13], [16] or the negative pressure [17], [18] were adopted to bend the substrate for the purposes of changing the orientation of MLA and expanding the FOV. Nevertheless, the fabrication process of such elements with enlarged FOV requires complicated experiment setups and rigorous environments controls.

For the efficient 3D micro-manufacture, an innovative maskless lithography technology [19]–[22] has been proposed to fabricate such structures like the Fresnel lens [21] and the hexagonal compound eyes [22]. The designed structures were horizontally sliced into several layers; each layer will be transformed into a virtual mask on the DMD chip to conduct the multi-layers lithography. Thus, the extra cost on the physical mask and the misalignment errors in the fabrication of multi-layers are reduced. Furthermore, to improve the accuracy of the surface profile of the fabricated structures, new slicing strategies e.g., equal-height slicing strategy [23] and equal-arc-mean slicing strategy [22] were presented. However, such methods required both the extra process of slicing layers and the multiple exposure time.

In this work, a modified dose modulated maskless lithography (DMML) is proposed for the one-step fabrication of a compound eyes array with enlarged FOV. The mechanism of dose modulated effect by the DMD was primarily analyzed to quantify the relations among the grayscale of pixels on the DMD, the corresponding exposure dose, and the corresponding exposure depth on photoresist. Then, a digital gray mask, which contains $1024*768$ pixels, was generated to control the exposure depth on the photoresist point-by-point. Finally the designed structure, a compound eyes array with specific orientation and enlarged FOV, was built in a one-step and simple exposure process. Because the DMML uses sequential gray-levels to modulate the exposure depth, the fabricated structure has a more continuous profile surface. Besides, the extra processes such as slicing processes or bending processes were also omitted.

2. The Principle of Dose-Modulated Effect

2.1 The Basic Setups and Principle

The basic experiment setups of DMML are shown in Fig. 1(a), of which the illumination system is used to provide the UV light-field with high-homogeneity at the wavelength of 365 nm. The DMD

chip (Wintech DLP 4100 0.7″ XGA, USA) contains 1024 × 768 micro-mirrors with each one at a size of 13.68 μm × 13.68 μm. This micro-mirror array can be regarded as a dynamic optic mask for the reason that each mirror can be independently rotated ±12°, which represents the "ON" or "OFF" status. Cooperated with a 6.75 × demagnifying optic projection lens, the minimum resolution at the imaging plane is nearly 2 μm.

Fig. 1(b) shows the basic principle of the dose-modulated effect. The DMD chip recognizes the gray-levels among 0 255 on the digital pattern, and saves it as 8-bit binary data. Based on the theory of pulse width modulation (PWM), the working time of each mirror can be independently controlled according to the binary data. Thus, the UV light can be modulated with different intensity by changing the grayscales on the digital pattern.

Because of the dose modulated effect aforementioned, the DMML uses a digital pattern, which contains 1024 × 768 pixels, to modulate the exposure depth on photoresist to form the three dimensional surface in a single step. Which means the DMD will modulate the whole light-field with required exposure dose distribution according to the grayscale information. As a result, different exposure depth appears in a single exposure process. This effect provides an efficient and low-cost way for the fabrication of complicate three-dimensional structures.

2.2 Calibration of the Dose-Modulated Effect

To build the required micro-structures on the photoresist, the analyzation of the dose modulated effect is essential. Only the relationships among the grayscale of pixels on DMD, the corresponding exposure dose, and the corresponding exposure depth are quantified, can we use the DMML method to form the continuous 3D structures in a one-step and simple way. Such effect can be divided into two factors, i.e., the exposure dose modulation on the DMD and the corresponding exposure depth on the photoresist.

Theoretically the relationship between the grayscale of pixel on DMD and its corresponding exposure dose should be a linear ratio for that the DMD modulates the exposure dose according to the PWM. However, little difference is always existed in the practical application among most DMD. Thus, we primarily quantified the dose modulation effect of the DMD in our lab before the fabrication process.

Generally, the exposure dose can be expressed by

$$E(x, y) = I(x, y) \times T \tag{1}$$

where $I(x, y)$ represents the intensity of incident light and T means the exposure time. The calculation shows that the exposure dose is in direct proportion to the exposure intensity while T is a constant. Therefore, the calibration of exposure dose can be replaced by the exposure intensity.

An ultraviolet intensity meter (UIT-250, USHIO Japan, Inc., Japan) was used to measure the UV light intensity while changing the grayscale on the virtual mask. The experiment data was shown in Fig. 2(a). It is noted that the intensity of grayscale below 50 is basically 0 mW/cm2, while it increases slowly for the lower gray levels. In contrast, the intensity increases rapidly for the grayscale over 160. This effect is due to the nonlinear control of PWM [24]. Besides, the error inflexion on the curve may be caused by the coding mistake of this DMD chip. Therefore, we adopted the steady-growing grayscale section from 50 to 150 (see Fig. 2(b)) to avoid the error section, which means the exposure intensity from 0.1 mW/cm2 to 3.5 mW/cm2.

Since the exposure dose can be controlled by changing the grayscale on the virtual mask, the properties of photoresist should be taken into consideration. The value of contrast γ between the exposure dose and the depth of photoresist [25] is shown below

$$\gamma = \frac{1}{lnE_{cl} - lnE_{th}} = \frac{D(x, y)/D_{total}}{lnE(x, y) - lnE_{th}} \tag{2}$$

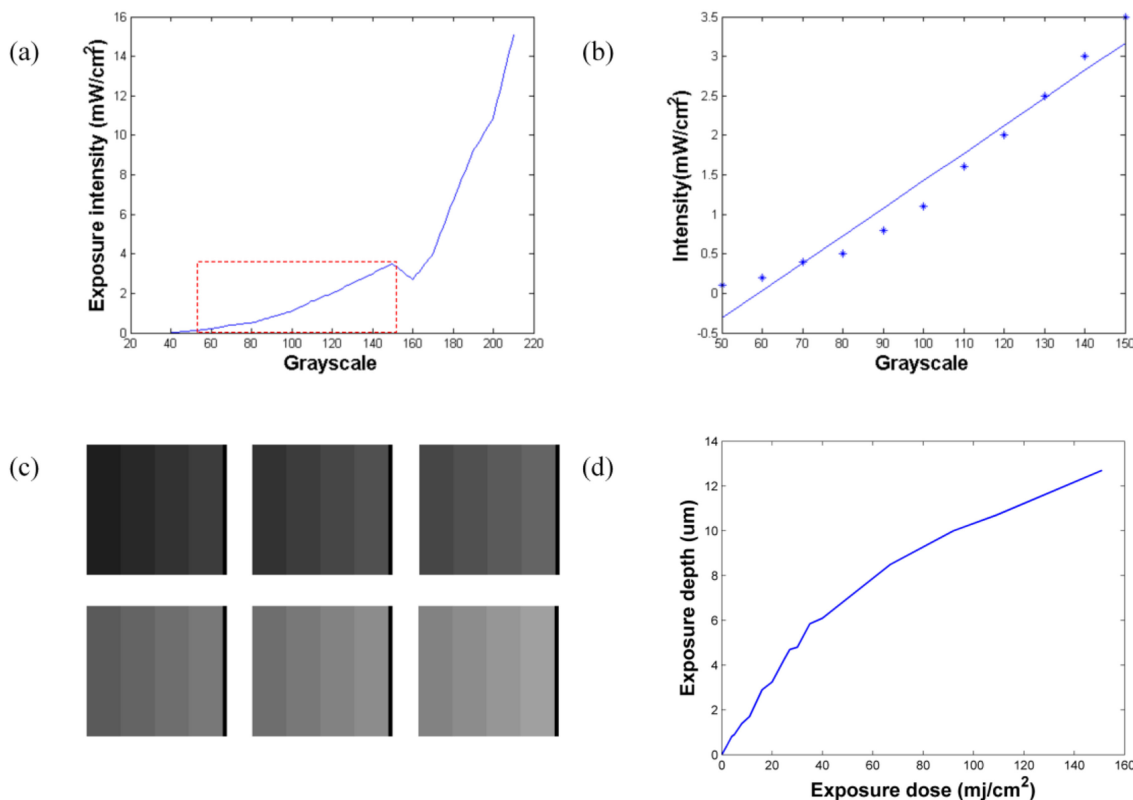where $0 < D(x, y) < T_{ph}$ and $E_{th} < E(x, y) < E_{cl}$.

Fig. 2. (a) Relationship curve between the grayscale on the virtual mask and the exposure intensity. (b) Details of grayscale among 50-150 which shows nearly linear distribution. (c) Virtual gray masks for the calibration between the exposure dose and the exposure depth. (d) The curve of exposure dose – exposure depth.

In this equation, $D(x, y)$ and D_{total} represent the exposure depth and the maximum thickness of photoresist, respectively. The E_{th} means the minimum exposure dose to start the reaction, and E_{cl} is the clear dose to react all the photoresist completely.

The following equation can be derived from equation (2)

$$E(x, y) = \exp\left(\frac{\gamma \times D_{total}}{D(x, y)}\right) + E_{th} \tag{3}$$

From the equation above, while the exposure dose is greater than the exposure threshold E_{th}, the photoresist will dissolve or solidify (depends on the properties of photoresist) in a nonlinear way. To clearly ensure this nonlinear reaction, an experiment about the exposure dose and depth was conducted. The AZ9260 positive photoresist was chosen as the recording materials coated on silica wafer for it can be spun to the maximum thickness at 15 μm. In the condition of 600 rpm slow rotation speed for 8 s and 2000 rpm for 50 s, the thickness of photoresist was nearly 10 μm. Next the wafer was put on a hotplate at 110 °C for 4 minutes in the prebake process, and 10 minutes in the dark box to cool down the wafer to the room temperature. The testing digital virtual grayscale masks were shown in Fig. 2(c), which contains several grayscale matrixes increased by 10 gray levels. The exposure time was fixed at 35 s for each virtual gray mask. Then the wafer was immersed in the development liquid which comprising the development solution AZ400K and the deionized water (1:1) for 45 s. The curve shown in Fig. 2(d), which illustrates the relationships between the exposure dose and the exposure depth, was obtained by scanning the development results under a step-profiler (DektakXT, Bruker, Karlsruhe, Germany) and smooth curve-fitting.
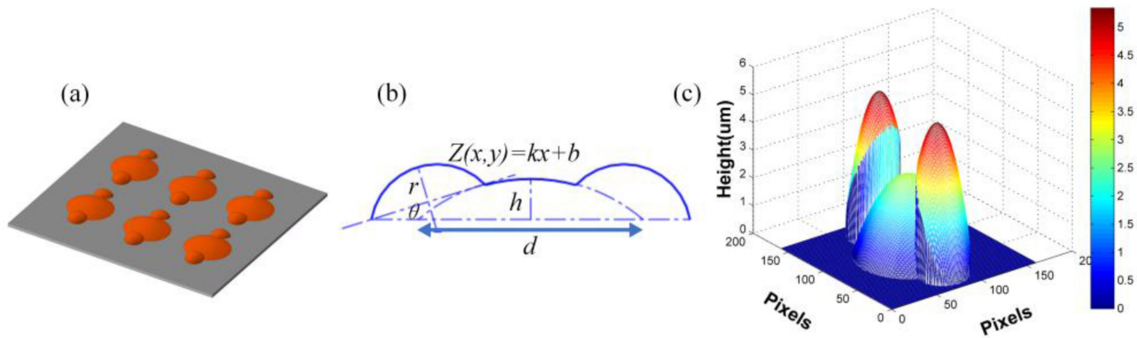
Fig. 3. (a) 3D model of designed compound eyes with individual orientation. (b) The mathematical model. (c) The required exposure depth on photoresist.

Combined with the relationship between grayscale on the virtual mask and the exposure dose (Fig. 2(a)), the actual exposure depth on the AZ9260 photoresist related to arbitrary grayscale of pixels on the DMD chip is confirmed. By precisely calculating the heights of each pixel on the designed structure and transferring them into grayscale information, the digital gray-mask can be generated and uploaded to the DMD, acting as a virtual mask to obtain the required distribution of exposure dose.

3. Fabrication of the Compound-Eyes Array

3.1 Digital Gray-Mask Generating

To obtain the required exposure dose distribution, the surface profile of the designed structure should be precisely calculated. Fig. 3(a) displays the sketch of the designed compound eyes, which is composed of two outer tilted microlens and one middle microlens. Instead of bending the planar substrate to change the orientation of MLA (aforementioned in Section 1), the symmetry axis of this outer microlens has a direct rotated angle in the design (Fig. 3(b)), which means they can receive information in a tilted angle.

The middle microlens of this compound eye (Fig. 3(b)), playing a role as a support structure, can be calculated by the bottom diameter d and maximum height h

$$z_0(x, y) = \sqrt{\left(\frac{h^2 + d^2}{2h}\right)^2 - x^2 - y^2} - \left(\frac{h^2 + d^2}{2h}\right) + h \qquad (4)$$

The outer tilted microlens can be regarded as a curve surface, generated by cutting the upper part of a sphere with an inclined plane. Thus, the mathematical equation contains the radius r, the linear parameter k and b

$$\begin{cases} z_1(x, y) = \sqrt{r^2 - x^2 - y^2} \\ z_1(x, y) \geq kx + b \end{cases} \qquad (5)$$

The rotated angle of outer microlens can be calculated as

$$\theta = \arctan \frac{k}{\beta} \qquad (6)$$

where β means the stretching parameter, calculated by the ratio between the ideal size of a single pixel in simulation and the actual exposure size of a single point on the photoresist. In this dose modulated maskless lithography method, the single pixel will be shrank to 2 μm (the minimum resolution). The linear parameter k is decided as 0.1. Therefore, the rotate angle θ should be 2.86° according to the eq. (6), which is basically satisfied to verify our fabrication method.
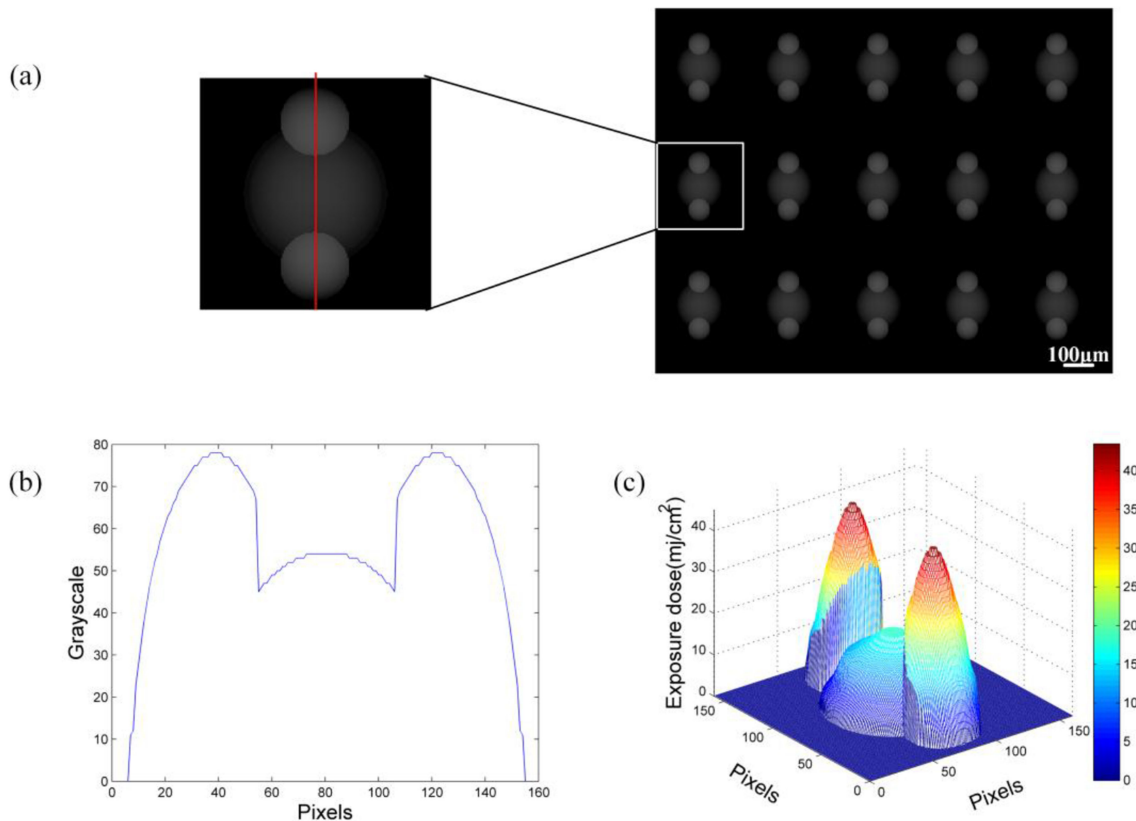
Fig. 4. (a) Gray-pattern of single compound eyes and the whole gray-mask at size 1024 × 768. (b) Cross-sectional grayscale information of single gray-pattern. (c) Exposure dose distribution of single gray-pattern.

To avoid the cross-talk caused by the adjacent microlens, the focal length of the inner and outer lens requires a little difference. In this design, the bottom diameter d and the maximum height h of the inner microlens were 200 μm and 3 μm respectively. The radius r of the outer microlens was calculated as 544 μm. The ideal focal length should be 1.9 mm for the outer microlens and 5.8 mm for the middle microlens. Based on the design data, simulated result of the exposure depth on photoresist was worked out through MATLAB (Ver.7.1, Natick, USA) and displayed in Fig. 3(c).

According to the quantification data of dose modulated effect aforementioned in Section 2.2, the required exposure depth can be represented by specific grayscale information in the DMML. In this way, the whole structure was transferred into a gray pattern. Following the pattern was expanded to 1024 × 768 size to fit the number of micro-mirrors on the DMD (Fig. 4(a)). Each pixel on this pattern will influence the exposure depth independently. Fig. 4(b) exhibits the cross-sectional grayscale information of the single digital pattern and Fig. 4(c) shows the simulated exposure dose distribution.

3.2 Fabrication Process

Since the designed digital gray pattern was generated and uploaded to the DMD chip as a virtual lithography mask, the fabrication process was basically the same as the experiments aforementioned (see section 2.2). Explicit procedures are displayed as 3D models in Fig. 5. The whole compound eyes array was transferred to photoresist in a single step due to the modulated dose distribution. Note that the optical field is formed by pixels, it still shows stairs under
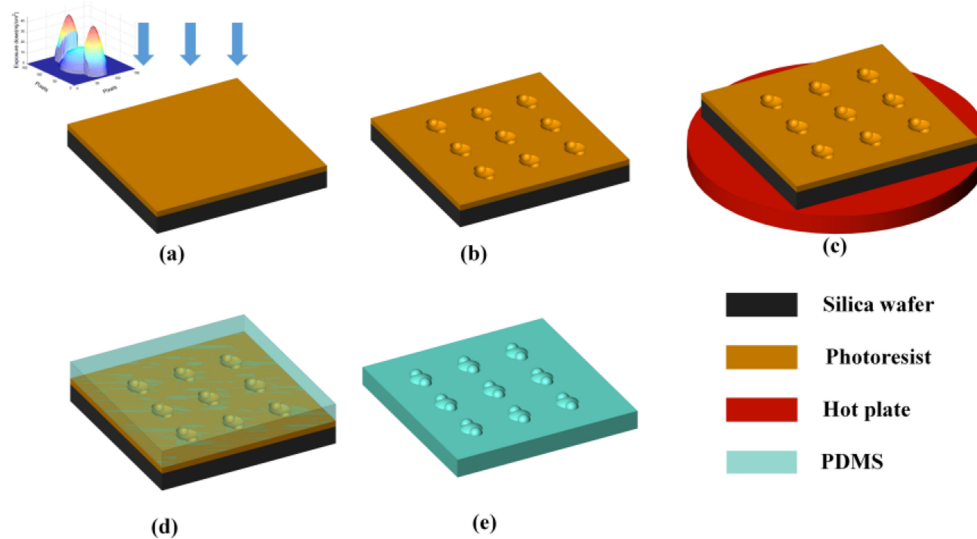
Fig. 5. Fabrication process which contains: (a) exposure process with modulated dose distribution, (b) development, (c) thermal reflow on a hot plate, (d) reversing pattern by PDMS, and (e) peeling off the PDMS film.

step-profiler. Therefore, we adopted the thermal reflow method (110 °C on the hotplate with full contact for 3 minutes) to slightly optimize such issue after the exposure process (see Fig. 5(c)). At the end of the fabrication procedure, polydimethylsiloxane (PDMS, mixed by prepolymer: curing agent = 1: 10) was used to reverse the pattern. After solidifying in the oven at 75 °C for 1 h and in the room temperature for 3 h to release bubbles, the PDMS film was peeled off from silica wafer with the thickness at nearly 6 mm (Fig. 5(d) and (e)).

4. Results and Discussions

In order to verify the fabrication result of the DMML, several experiments were conducted to quantify if the physical performance of the fabricated compound eyes is coincident with our design or not.

Fig. 6(a) displays the pictures of the fabrication result. The precise surface profile under step-profiler is shown in Fig. 6(b), which contains three cross-sectional curves: the exposure curve, the thermal reflow curve, and the design curve. The exposure profile and the design profile are similar at the outer surface, which means this method exhibits an excellent ability on the fabrication of continuous 3D surface. The main deviation appears in the middle part, which should be the reason that the middle part has a smoother surface than the outer part, and less gray-levels were applied in the digital gray pattern. In summary, the resulting profile of the fabricated compound eyes is basically consistent with our design profile.

Although the profile surface of the fabricated result is similar to the design data, we still did other experiments to verify the optical abilities. We have introduced that the focal length of the middle microlens and the outer microlens should keep little difference to avoid the optical cross-talk. In this design, the ideal focal length is 1.9 mm for the outer microlens and 5.8 mm for the middle microlens. The test platform shown in Fig. 7 was used to test this data. The object was illuminated by a white light source; then the light was focused by the compound eyes. A microscope lens (Nikon, Plan flour, 10X/0.3, WD = 16 mm, Japan) captured the virtual images and transferred them to the CCD camera (WAT-902 H).

The quartz glass with line pattern shown in Fig. 8(a) was used as object, of which the yellow part is coated with opaque chromium layer. The distance (l) between the lithography mask and the compound eyes array was nearly 200 mm. From the lens imaging equation (eq. 7), the imaging
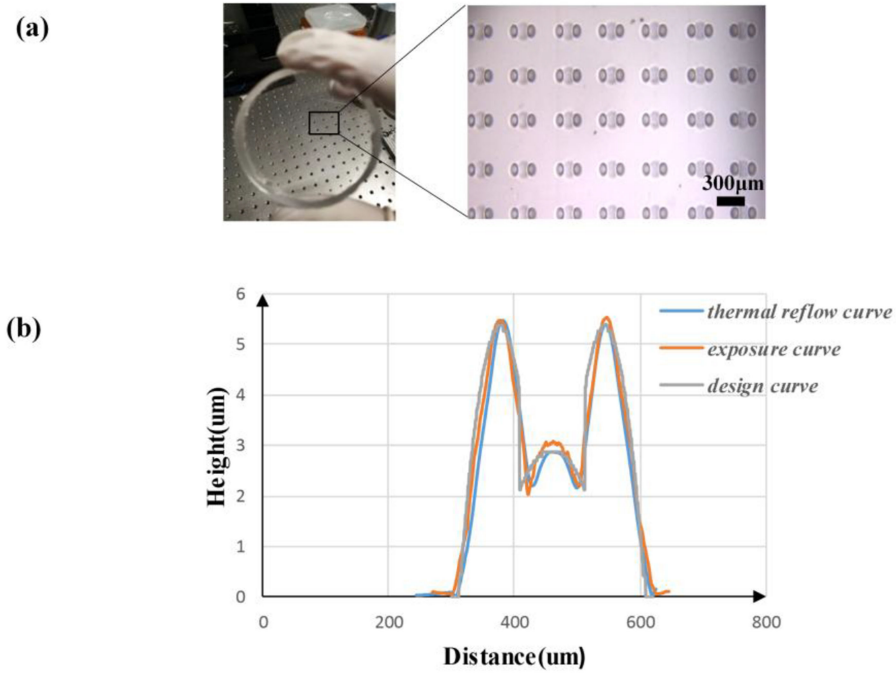
Fig. 6. (a) Fabrication result and magnifying picture under a microscope. (b) Profile surface under step-profiler with: exposure curve, thermal reflow curve, and design curve.
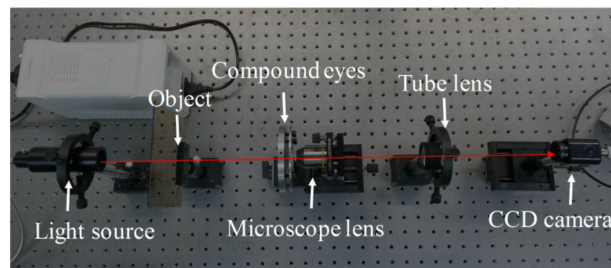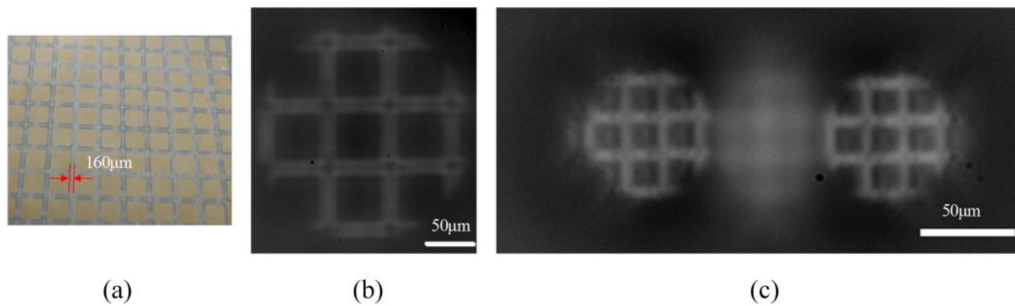

Fig. 7. Optic experiment platform.

Fig. 8. (a) Lithography mask applied as an object with minimum features at 160 μm. And patterns captured by (b) middle microlens and (c) outer microlens.
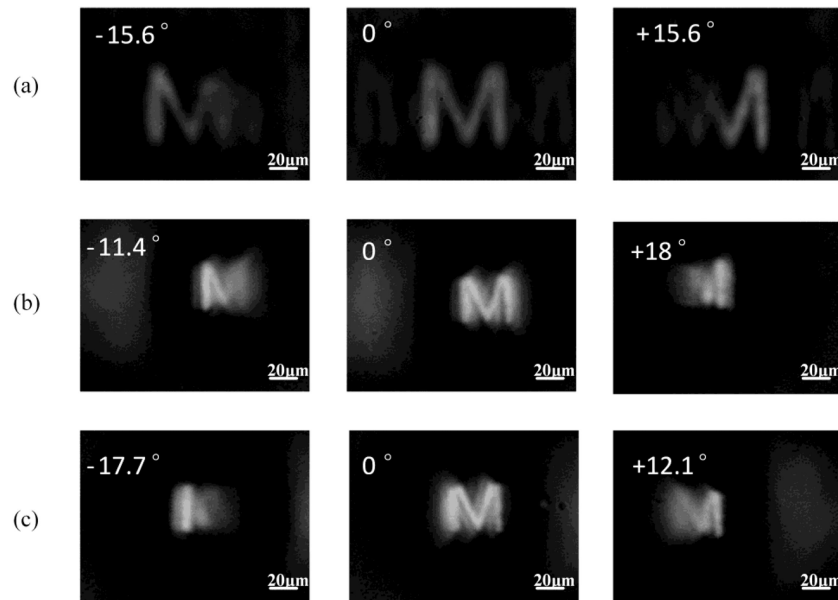
Fig. 9. Images captured at different angle by: (a) the middle microlens, (b) the right microlens, and (c) the left microlens.

length (l') of the outer microlens and the middle microlens were calculated as nearly 1.8 mm and 5 mm, respectively.

$$\frac{n'}{l'} - \frac{n}{l} = \frac{n' - n}{r} \qquad (7)$$

By moving the microscope lens along the axis of the optical system, the clearest pattern was captured at nearly d = 17 mm (Fig. 8(b)) for the middle microlens and nearly d = 20.5 mm for the outer microlens (Fig. 8(c)), in which the distance d contains the image distance of fabricated compound eyes array and the working distance of the microscope lens. The deviation between the ideal data and the actual result is in the range of focal depth.

Furthermore, we set up another imaging experiment to verify the rotated orientation of the outer microlens. A hand-cut letter 'M' was used as the observed object placed at 200 mm in front of the fabricated compound eyes. Thus the gap between two adjacent microlens (nearly 200 μm) was inconsequential. In this experiment, we tested the angle that half of the letter 'M' can be seen to evaluate this rotated angle.

Final experiment results of the same ommatidium are shown in Fig. 9. The angle of half of the letter 'M' can be clearly seen through the middle microlens is approximately $\pm 15.6°$ (Fig. 9(a)). The symmetrical data means that the middle microlens has a similar performance with the normal microlens. Besides, the angle is nearly from $-11.4°$ to $+18°$ for the right microlens (Fig. 9(b)) and nearly from $-17.7°$ to $+12.1°$ for the left microlens (Fig. 9(c)), which means that the whole view angle is from $-17.7°$ to $+18°$. It can be deduced that the orientation of each outer microlens was rotated for nearly 3° around the vertical optic axis, which was basically the same with our design. The experiment data revealed that the fabricated planar compound eyes exhibits specific orientation and it should have an enlarged FOV.

5. Conclusion

In this work, a DMML method is proposed to fabricate a special compound eyes array with specific orientation on a planar substrate. For the precise fabrication of such structure, we quantified the

relationships among the grayscale on the virtual mask, the exposure dose and the exposure depth. Then, we generated a virtual mask, which contains 1024×768 pixels, to control the exposure depth on the photoresist point-by-point to form the required structure. In this way, the compound eyes, with an aperture at nearly 300 μm, a maximum height at nearly 6 μm, and enlarged FOV, was transferred on the photoresist with a continuous surface in one-step exposure, which avoids the complicated fabrication setups and rigorous environments. The surface profile of the fabricated compound eyes measured by step-profiler has a great agreement as our design. Additionally, PDMS was adopted to reverse the model pattern on wafer for the further optical experiment, including focal length and rotated orientation; the final results show little aberration with the ideal data, which represent that the dose-modulated lithography is effective and convenient for the fabrication of continuous surface such as this compound eyes with enlarged FOV or other mirco-devices with complicate surface.

References

[1] K. Seong-Weon and R. S. Ramakrishna, "Simultaneous 360 degrees viewing optical system with the lenses of the compound eyes from the dragonfly," *Proc. SPIE*, vol. 6624, Mar. 12, 2008, Art. no. 662402.

[2] M. Kaya, I. Sargin, I. Al-jaf, S. Erdogan, and G. Arslan, "Characteristics of corneal lens chitin in dragonfly compound eyes," *Int. J. Biol. Macromolecules*, vol. 89, pp. 54–61, Aug. 2016.

[3] Y. M. Song *et al.*, "Digital cameras with designs inspired by the arthropod eye," *Nature*, vol. 497, no. 7447, pp. 95–99, May 2013.

[4] H. Chen, X. Shen, X. Li, and Y. Jin, "Bionic mosaic method of panoramic image based on compound eye of fly," *J. Bionic Eng.*, vol. 8, no. 4, pp. 440–448, Dec. 2011.

[5] D. Keum, H. Jung, and K.-H. Jeong, "Planar emulation of natural compound eyes," *Small*, vol. 8, no. 14, pp. 2169–2173, Jul. 2012.

[6] Y. Dong and J. Liu, "Motion detection based on curved artificial compound eyes," *Sens. Mater.*, vol. 27, no. 11, pp. 1131–1135, 2015.

[7] H. Kawano *et al.*, "Practical design for compact image scanner with large depth of field by compound eye system," *Opt. Express*, vol. 22, no. 15, pp. 18010–18019, Jul. 2014.

[8] K. H. Jeong, J. Kim, and L. P. Lee, "Biologically inspired artificial compound eyes," *Sci.*, vol. 312, no. 5773, pp. 557–561, Apr. 2006.

[9] D. Floreano *et al.*, "Miniature curved artificial compound eyes," *Proc. Nat. Acad. Sci. USA*, vol. 110, no. 23, pp. 9267–9272, Jun. 2013.

[10] K. Yoshimoto *et al.*, "Gastrointestinal tract volume measurement method using a compound eye type endoscope," *Proc. SPIE*, vol. 9313, Mar. 4, 2015, Art. no. 93131I.

[11] H. K. Raut *et al.*, "Multiscale ommatidial arrays with broadband and omnidirectional antireflection and antifogging properties by sacrificial layer mediated nanoimprinting," *ACS Nano*, vol. 9, no. 2, pp. 1305–1314, Feb. 2015.

[12] K. Kagawa *et al.*, "An active intraoral shape measurement scheme using a compact compound-eye camera with integrated pattern projectors," *Japanese J. Appl. Phys.*, vol. 48, no. 9, Sep. 2009, Art. no. 09lb04.

[13] Z. Deng *et al.*, "Dragonfly-eye-inspired artificial compound eyes with sophisticated imaging," *Adv. Functional Mater.*, vol. 26, no. 12, pp. 1995–2001, Mar. 2016.

[14] X. Gao *et al.*, "The dry-style antifogging properties of mosquito compound eyes and artificial analogues prepared by soft lithography," *Adv. Mater.*, vol. 19, no. 17, pp. 2213–2217, Sep. 2007.

[15] A. Cao *et al.*, "Design and fabrication of a multifocal bionic compound eye for imaging," *Bioinspiration Biomimetics*, vol. 13, no. 2, Mar. 2018, Art. no. 026012.

[16] W.-K. Kuo, S.-Y. Lin, S.-W. Hsu, and H. H. Yu, "Fabrication and investigation of the bionic curved visual microlens array films," *Opt. Mater.*, vol. 66, pp. 630–639, Apr. 2017.

[17] J. Luo, Y. Guo, and X. Wang, "Rapid fabrication of curved microlens array using the 3D printing mold," *Optik*, vol. 156, pp. 556–563, 2018.

[18] J. Luo, Y. Guo, X. Wang, and F. Fan, "Design and fabrication of a multi-focusing artificial compound eyes with negative meniscus substrate," *J. Micromech. Microeng.*, vol. 27, no. 4, Apr. 2017, Art. no. 045011.

[19] W. Iwasaki *et al.*, "Maskless lithographic fine patterning on deeply etched or slanted surfaces, and grayscale lithography, using newly developed digital mirror device lithography equipment," *Japanese J. Appl. Phys.*, vol. 51, no. 6, Jun. 2012, Art. no. 06fb05.

[20] K. F. Chan, Z. Q. Feng, R. Yang, A. Ishikawa, and W. H. Mei, "High-resolution maskless lithography," *J. Microlithography Microfabr. Microsyst.*, vol. 2, no. 4, pp. 331–339, Oct. 2003.

[21] S. L. Aristizabal *et al.*, "Microlens array fabricated by a low-cost grayscale lithography maskless system," *Opt. Eng.*, vol. 52, no. 12, Dec. 2013, Art. no. 125101.

[22] B. Yang, J. Zhou, Q. Chen, L. Lei, and K. Wen, "Fabrication of hexagonal compound eye microlens array using DMD-based lithography with dose modulation," *Opt. Express*, vol. 26, no. 22, pp. 28927–28937, Oct. 2018.

[23] J.-W. Choi, R. B. Wicker, S.-H. Cho, C.-S. Ha, and S.-H. Lee, "Cure depth control for complex 3D microstructure fabrication in dynamic mask projection microstereolithography," *Rapid Prototyping J.*, vol. 15, no. 1, pp. 59–70, 2009.

[24] Q. Deng, Y. Yang, H. Gao, Y. Zhou, Y. He, and S. Hu, "Fabrication of micro-optics elements with arbitrary surface profiles based on one-step maskless grayscale lithography," *Micromach.*, vol. 8, no. 10, Oct. 2017, Art. no. 314.

[25] H. Kemhadjian, "Microlithography: Science and Technology," *Int. J. Elect. Eng. Educ.*, pp. 275–276, 2007.